

Mixed Fluid Conditions: Capillary Phenomena

J. C. Santamarina¹ and Z. Sun²

¹ KAUST, Thuwal, Kingdom of Saudi Arabia, carlos.santamarina@kaust.edu.sa

² KAUST, Thuwal, Kingdom of Saudi Arabia, zhonghao.sun@kaust.edu.sa

ABSTRACT

Mixed fluid phenomena in porous media have profound implications on soil-atmosphere interaction, energy geotechnology, environmental engineering and infrastructure design. Surface tension varies with pressure, temperature, solute concentration, and surfactant concentration; on the other hand, the contact angle responds to interfacial tensions, surface topography, invasion velocity, and chemical interactions. Interfaces are not isolated but interact through the fluid pressure and respond to external fields. Jumps, snap-offs and percolating wetting liquids along edges and crevices are ubiquitous in real, non-cylindrical porous networks. Pore- and macroscale instabilities together with pore structure variability-and-correlation favor fluid trapping and hinder recovery efficiency. The saturation-pressure characteristic curve is affected by the saturation-history, flow-rate, the mechanical response of the porous medium, and time-dependent reactive and diffusive processes; in addition, there are salient differences between unsaturation by internal gas nucleation and gas invasion. Capillary forces add to other skeletal forces in the porous medium and can generate open-mode discontinuities when the capillary entry pressure is high relative to the effective stress. Time emerges as an important variable in mixed-fluid conditions and common quasi-static analyses may fail to capture the system response.

INTRODUCTION

Multiphase fluids are ubiquitous in porous media and play a critical role in a wide range of applications, such as infrastructure, resource recovery, agriculture, atmosphere-subsurface interaction, and biological systems. Examples from the field of energy-geoengineering include: oil and gas recovery, contamination by non-aqueous phase liquids NAPL and environmental remediation (dense DNAPL: heavy oils, coal tars; light LNAPL: gasoline and supercritical CO₂), methane hydrate bearing sediments, geological storage of CO₂ and backfill in nuclear waste repositories. These examples involve gases (air, vapor, methane), supercritical fluids (e.g., CO₂), liquids (water, brine, oil and contaminants), and even solids (e.g., hydrate).

Capillary phenomena in porous media control the distribution of phases and residual saturation, determine the relative permeability and flow regimes, impact effective stress and mechanical properties of porous media, and are responsible for a wide range of emergent

phenomena – from lung collapse to desiccation cracks in mud ponds. Although the basic laws of capillarity are well understood, complexities arise in porous media and natural systems, in part due to multi-scale geometric effects and physical couplings. The purpose of this manuscript is to explore the wealth of capillary phenomena in porous media and to identify emergent characteristics with emphasis on energy geo-engineering applications.

FUNDAMENTAL CONCEPTS

Two contiguous phases in equilibrium experience incessant jumping of molecules from one phase to the other (limited by their mutual solubilities), and differences in attractive molecular interactions within each phase. These apply to all mixed-phase systems such as air-water, methane-water, brine-oil and hydrate-water.

Surface/Interfacial Tension. Surface tension results from differences in attractive interactions that occur between molecules at the interface and molecules within the bulk fluids away from the interface (Figure 1a). Surface tension T_s is the work per unit area required to increase the interface area [J/m^2] or the force per unit length the interfacial “membrane” exerts [N/m].

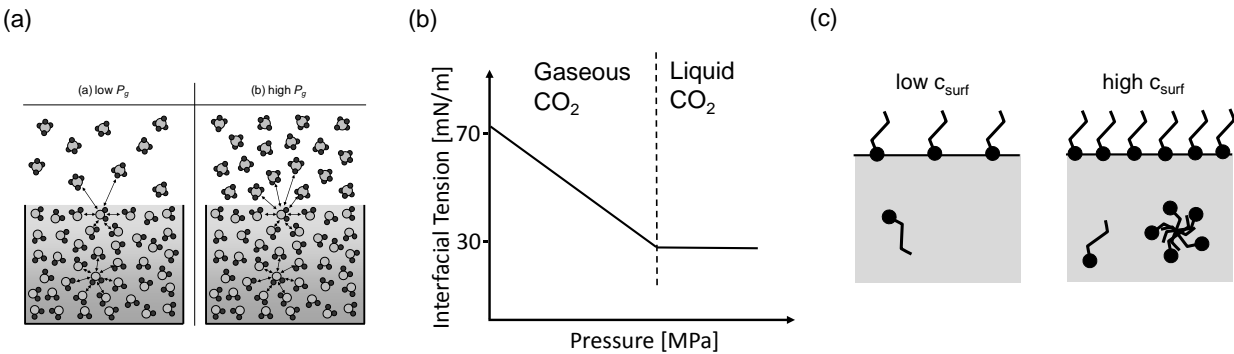


Figure 1. Interfacial tension. (a) Molecular-scale attractive interactions. (b) Pressure dependency in gas-liquid systems [data in Espinoza and Santamarina, 2010]. (c) The effect of surfactants.

Temperature. In general, the surface tension decreases with the increase in temperature due to the increased molecular vibration relative to attraction forces. An asymptotic linear trend describes changes near stable conditions $T_s = \alpha - \tau T$. For example, the rate of change is $\tau = 0.1477$ (mN/m)/°C for air-water surface tension at $p = 1$ atm [Jasper, 1972]. Some water-alcohol mixtures exhibit surface tension that increases with temperature [Karapetsas et al., 2014].

Pressure. Higher gas pressure implies higher gas density and molecular attractive interactions at the interface. Hence, the gas-liquid interfacial tension decreases with increasing gas pressure, and remains fairly constant once the gas liquefies at the vapor-liquid boundary (Figure 1b). For example, the interfacial tension for water-CO₂ at 25°C is [Massoudi and King, 1974; see Chalbaod et al., 2009 for brine-CO₂]:

$$T_s [mN / m] = 71.98 - 0.7789 u_{CO_2} / atm + 0.00543 u_{CO_2}^2 / atm^2 - 0.000042 u_{CO_2}^3 / atm^3$$

Salt. The gas-water interfacial tension increases with salt concentration because of increased attractive interactions among hydrated ions in the water solution. The asymptotic change in surface tension at low salt concentration $c < 1$ M is a linear trend $T_s = \alpha + \chi \cdot c$; for example, the rate of change is $\chi = 1.55$ (mN/m)/M for NaCl solution [Weissenborn and Pugh, 1996; see Chalbaud et al., 2009 for brine-CO₂].

Surfactants. “Surface active agents” have an amphipathic structure with both hydrophobic and hydrophilic ends so they tend to migrate towards interphases (Figure 1c). Surfactants that remain in the bulk solution eventually form micelles when the concentration reaches the critical micelle concentration CMC. Surfactants at the interface align and repel each other decreasing the surface tension. Hence, the interfacial tension decreases with surfactant concentration until excess surfactants in the bulk solution form micelles beyond the CMC [Holmberg et al., 2003; Rosen, 2004; Israelachvili, 2011].

Excess charges. Water can gain excess charge by charge separation between water and the solid surface [Choi et al., 2013]. Excess charges repel each other and migrate towards the droplet outer surface where their repulsion causes a decrease in the surface tension proportional to the surface charge [experimental evidence in Santos et al., 2011].

Marangoni effect. Sudden changes in surface concentration or temperature cause transient gradients in the surface tension, and the interfacial membrane contracts towards the area with the higher surface tension.

Time-dependent changes. The interfacial tension adjusts as fluids dissolve into each other until they reach equilibrium. For example, the initial interfacial tension of water-air decreases by almost 20% in a water-benzene-air system as benzene dissolves in water.

Wettability and Contact Angle. Wettability is the relative affinity that interacting fluids exhibit towards a solid substrate. The contact angle θ the fluid interface defines against the solid surface characterizes wettability, and it captures the force-equilibrium among the interfacial tensions that arise between the fluids V and L and the solid S [Figure 2a]:

$$\cos \theta = \frac{T_{VS} - T_{LS}}{T_{LV}} \quad \text{Young's equation}$$

The fluid on the lower side of the LV-interface is more affine to the solid.

Spreading coefficient. Consider a three-fluid system, such as air-oil-water. An oil droplet may spread on water to form a thin oil slick on the ocean surface, or a thin oil film around water-wet pores as air invades the porous medium. The spreading coefficient captures the balance between interfacial tensions in this three-fluid system (o=oil, w=water, and a=air – Figure 2b):

$$C_S = T_{aw} - (T_{ow} + T_{ao})$$

Oil will spread as a thin film between air and water when $C_S > 0$. If $C_S < 0$, the three phases reach equilibrium at a contact angle θ [Zhou and Blunt, 1997]. Oil production by gas-enhanced gravity drainage presumes oil spreading within the pores of water-wet reservoirs [Blunt et al., 1995].

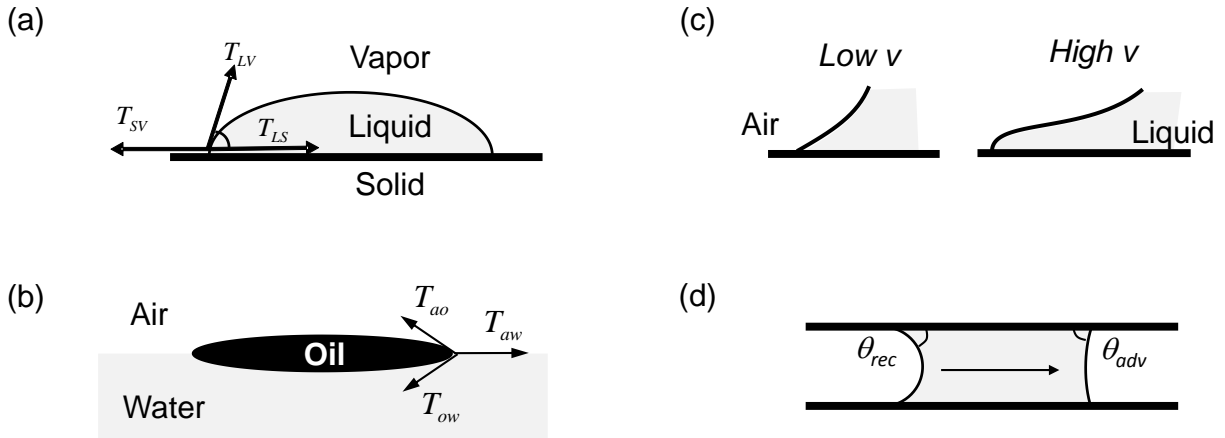


Figure 2. Contact angle. (a) Equilibrium between interfacial tensions between two fluids and a solid substrate. (b) Spreading in three-fluid system. (c) Dynamic effects. (d) Hysteresis.

Surface tensions - Pressure. Changes in interfacial tension discussed in the previous section affect the contact angle in agreement with Young's equation. This is readily seen in liquid-gas-mineral systems such as water-CO₂-mineral and water-CH₄-mineral where the gas-liquid interfacial tension T_{LV} decreases with gas pressure [data in Espinoza and Santamarina, 2010].

Dynamic contact angle. The contact angle is velocity-dependent; in particular, the advancing contact angle increases as the velocity increases [Figure 2c – data in Sobolev et al., 2000]. Molecular-scale explanations consider the kinetics of molecular attachment and detachment. Hydrodynamic explanations take into consideration viscous dissipation near the contact line and remnant films [Blake, 2006; Snoeijer and Andreotti, 2013]. A wetting transition takes place when the invading fluid advances at a high speed and a film of the defending fluid remains behind [Podgorski et al., 2001; Snoeijer and Andreotti, 2013; Hsu and Hilpert, 2015].

Contact angle hysteresis - Changes in wettability. Typically, the contact angle is different when the interface advances or recedes (Figure 2d). Underlying processes can be both chemical (changes in the surface chemistry during invasion and preferential adsorption of species) and geometrical features that can “pin” the contact line at submicron-scale surface roughness and heterogeneities [Butt et al., 2003; de Gennes et al., 2004; Quere, 2008]. Mineral surfaces tend to be water-wet relative to organic liquids and gases. However, wettability can change with the selective absorption of chemical compounds in oil and brines (e.g., surfactants, resins and asphaltenes). Temperature and pressure conditions (unclear trends - Buckley et al., 2001), time and kinetic rates and the saturation history affect trends [Kovscek et al., 1993; Powers and Tamblin, 1995; Powers et al., 1996; Buckley et al., 1998; Francisca and Santamarina, 2003; Drummond and Israelachvili, 2004; Abdallah et al., 2007].

Capillarity. The tensile membrane that separates two fluids can sustain a pressure difference. From force equilibrium, the pressure difference or capillary pressure Δu is proportional to the interfacial tension T_{LV} and the contact angle θ (Young-Laplace equation):

$$\Delta u = u_v - u_L = T_{LV} \cos \theta \left(\frac{1}{r_1} + \frac{1}{r_2} \right)$$

where the interface curvature has two principal radii r_1 and r_2 .

Interacting Menisci. Interfaces in porous media are not isolated; in fact, all menisci are interconnected through the fluid phase. Analytical and experimental results support the following observations [Alvarellos, 2003]: (1) Contact angles θ_i at interacting menisci are not constant but vary between the upper and lower bound contact angles established at the verge of advancing and receding motions, $\theta_{rec} \leq \theta_i \leq \theta_{adv}$. (2) Menisci respond to external forces within this range of contact angles. (3) Menisci geometry throughout the medium minimize the total energy.

For example, consider a droplet of a wetting fluid in a capillary tube (Figure 3a). If the tube lies flat, contact angles are the same at both ends, the value is within the range $\theta_{rec} \leq \theta_i \leq \theta_{adv}$ depending on the droplet formation history. As the tube is inclined, gravity adds the droplet self-weight, the contact angle at the lower end starts evolving towards θ_{adv} and towards the receding θ_{rec} at the upper end. The limiting values θ_{adv} and θ_{rec} determine the maximum biasing force the droplet can exert (a function of self-weight and inclination). Clearly, the droplet in an inclined tube is inherently unstable in the absence of contact angle hysteresis $\theta_{adv} = \theta_{rec}$ [Alvarellos, 2003].

Interaction through the vapor pressure. Liquids are in equilibrium with their vapor at LV interfaces. The vapor pressure at equilibrium u_v is curvature r dependent [Kalikmanov, 2013]:

$$\ln \left(\frac{u_v}{u_{sat}} \right) = \frac{2T_s \Omega}{k_B T r} \quad \text{Laplace-Kelvin equation}$$

where u_{sat} is the saturated vapor pressure for the bulk liquid, Ω the liquid molecular volume, $k_B = 1.38 \times 10^{-23}$ J/K is Boltzmann's constant, and T is temperature. Differences in equilibrium vapor pressure promote mass transport between pores of different sizes and wettability, as indicated in Figure 3b; this is a form of Ostwald ripening. Depending on pore size and geometry, water may fill small cavities and form plugs at pore throats leaving isolated inner and larger pores; this contributes to hysteresis during adsorption and desorption [Camuffo, 1984].

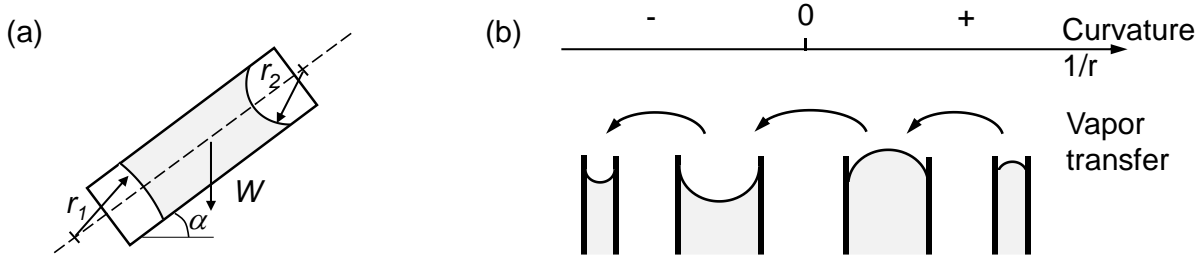


Figure 3. Interacting menisci. (a) Response to external bias (b) Interaction through vapor pressure.

PORE GEOMETRY

Models based on cylindrical pore geometries capture the prevalent role of pore size on mixed fluids in porous media. However, these models fail to represent other important phenomena that result from the non-cylindrical longitudinal and transverse geometry of natural pores.

Longitudinal Pore Geometry. Pervious porous media consist of concatenated pore throats-and-bodies (e.g., sediments and rocks) or lacunae-and-canalliculi (e.g., bones). Let's consider a sinusoidal pore throat geometry. Figure 4a presents the change in capillary pressure computed using the Young-Laplace equation as the fluid interface transverses the pore throat. In all cases, capillary pressure scales with surface tension, however, it is the contact angle that plays a more critical role: the interface may jump from concave-to-convex for intermediate contact angles with an associated reversal in capillary pressure. In fact, a partially wetting fluid may have to be “pushed” to go beyond the pore throat. Note that pressure maxima or minima do not occur at the pore throat except when $\theta=0$.

Pore Geometry and Surfactants. Transient changes in the surfactant surface density when the interface traverses the pore throat alter the interfacial response; then, the measured capillary pressures deviate from values predicted using the bulk surfactant concentration [Jang et al., 2016]. Similar transient changes underlie the role of surfactant self-regulation during pulmonary expansion and contraction [Clements et al., 1958].

Transverse Pore Geometry. Laplacian capillarity anticipates remnant wetting fluids in small pores, corners, crevices and edges after the pore has been invaded by a non-wetting fluid. Therefore, the wetting phase is prone to remain connected in porous media even at relatively high capillary pressures. Phase connectivity has important implications for fluid transport [Roof, 1970; Arriola et al., 1983; Ransohoff and Radke, 1988a; Dong and Chatzis, 1995; Bico and Quere, 2002]

Corners. Figure 4b shows a wetting fluid resting along corners. The Mayer and Stowe-Princen MS-P solution predicts the pressure difference Δu between the non-wetting fluid and the remnant wetting fluid at corners in terms of the perimeter of the contact line between the nonwetting fluid and the solid p_s , the perimeter of the contact line between the non-wetting fluid and the wetting fluid p_γ , and the cross-section area of the non-wetting fluid A_{eff} [Mason and Morrow, 1991; Ma et al., 1996; Mason and Morrow, 1994; Lago and Araujo, 2001]:

$$\Delta u = \frac{T_{LV}(p_s \cos \theta + p_\gamma)}{A_{eff}}$$

Edges. The fluid interface can be stable at various contact angles when the solid surface has high curvature at edges. This implies a range of possible capillary pressures for equilibrium when edges are present [Figure 4c; Morrow, 1970].

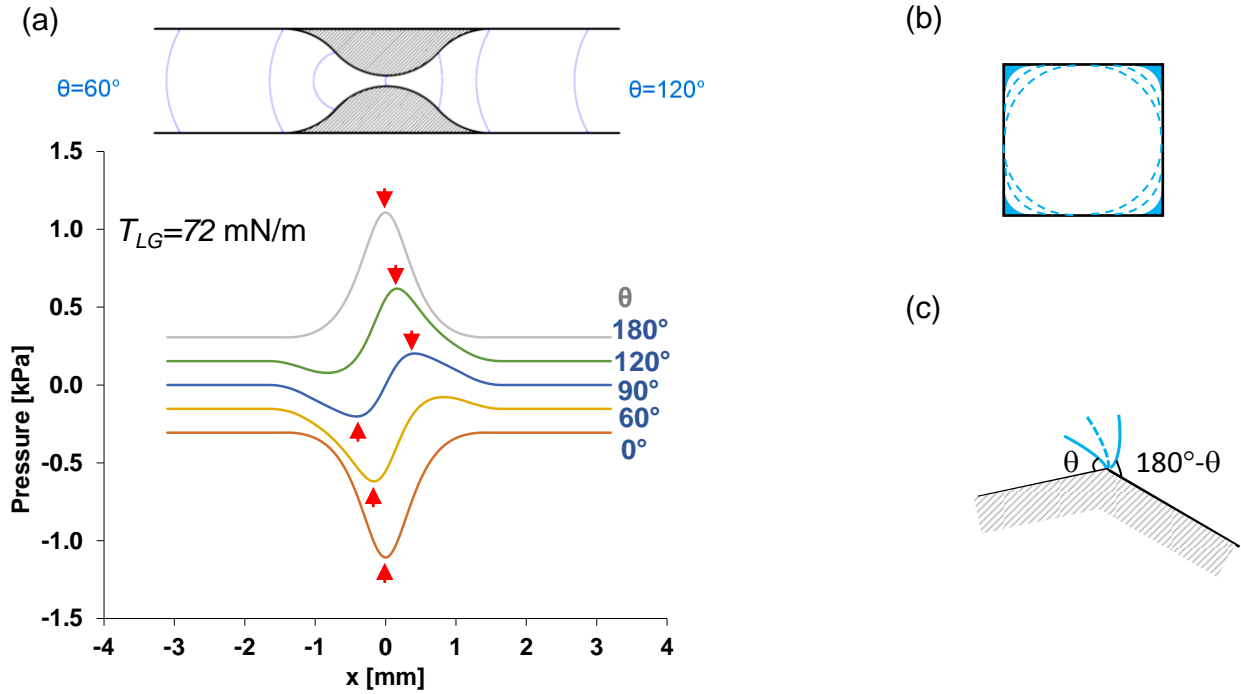


Figure 4. Pore geometry. (a) Longitudinal variation [Jang et al., 2016]. (b) Transverse variation. (c) Contact angle at edges.

INSTABILITIES

Pore-scale Instabilities. Pore geometry and capillary phenomena combine to give rise to various accelerations and instabilities as the fluid interface approaches or recedes away from a pore throat. These instabilities are associated with sudden changes in capillary pressure and often result in phase separation and entrainment [Figure 5a; Jang et al., 2016]:

- *Haines jump.* Spontaneous fluid redistribution after a sudden pressure change [Morrow, 1970; Mohanty et al., 1987; Gauglitz and Radke, 1989; Berg et al., 2013].
- *Snap-off/choke-off.* A wetting fluid plug forms at a pore throat and splits the traversing non-wetting fluid. Plugs may involve wetting fluids transported along corners and crevices or left behind during sudden jumps [Roof, 1970; Wardlaw, 1982; Arriola et al., 1983; Yu and Wardlaw, 1986a, b; Pena et al., 2009].
- *Lamellae and foam generation* due to repeated snap-offs [Ransohoff and Radke, 1988b; Rossen, 2003].

These instabilities contribute to fluid trapping during displacement, whereby a single displacement front becomes a multi-interface front, overall flow is hindered, and measured capillary pressures deviate from theoretically predicted values and become system-dependent [Lenormand et al., 1983].

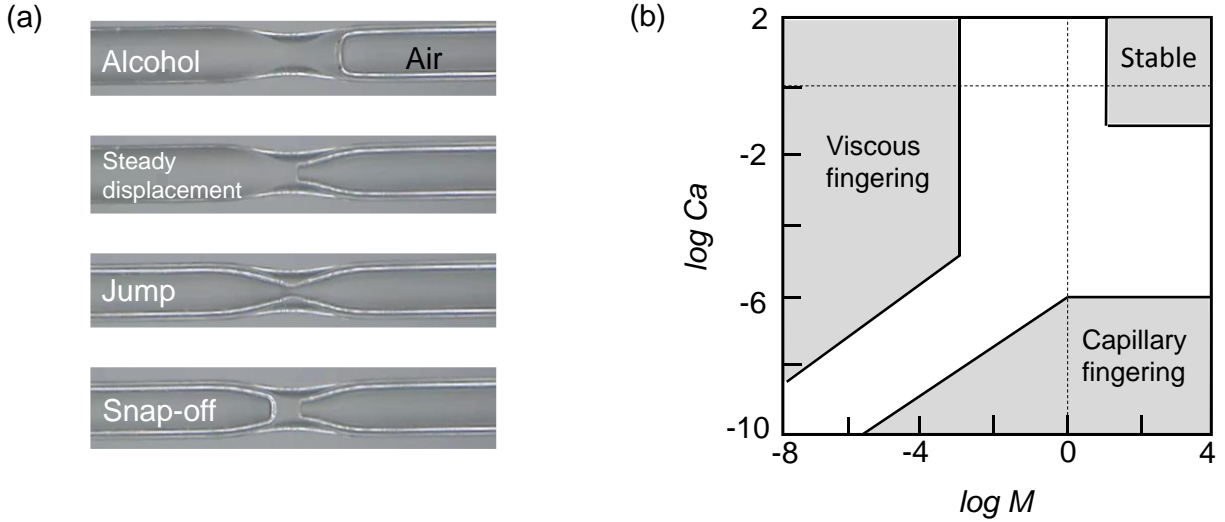


Figure 5. Instabilities. (a) Pore-scale: jumps and snap-offs. (b) Macro-scale: fingered invasion [Schematic – after Lenormand et al., 1988].

Macro-scale Instabilities. Consider an invading fluid advancing into a porous medium saturated with a defending fluid. The invasion pattern reflects wettability, mass densities, and viscosities. These parameters are captured in dimensionless ratios between capillary F_c , drag F_d and buoyant F_b forces:

$$\text{Capillary Number: } Ca = \mu_{inv} v / T_S$$

$$\text{Viscosity Ratio: } M = \mu_{inv} / \mu_{def}$$

Figure 5b illustrates different displacement regimes: stable displacement, viscous fingering and capillary fingering. Experimental and numerical studies show that the boundaries between the various invasion regimes are system-dependent [Lenormand et al., 1988; Zhang et al., 2011].

PRESSURE-SATURATION CHARACTERISTIC CURVE

The capillary pressure-saturation relationship, also known as the soil-water characteristic curve or soil water retention curve, defines the relationship between capillary pressure and the degree of saturation. This relationship plays a central role in modeling unsaturated soil behavior. Pressure-saturation data contains information that relates to the pore size distribution, pore connectivity and spatial correlation. Consequently, the characteristic curve affects the evolution of relative permeabilities, resource recovery, mechanical stability and deformation [Brooks and Corey, 1964; van Genuchten, 1980; Fredlund, 2000].

The pressure-saturation characteristic curve rests between two bounds. The lower bound corresponds to the pressure required for the non-wetting fluid to invade all pores aligned in series according to size starting from the largest pore. The upper bound is defined by the pressure required to invade the smallest pore [Figure 6a].

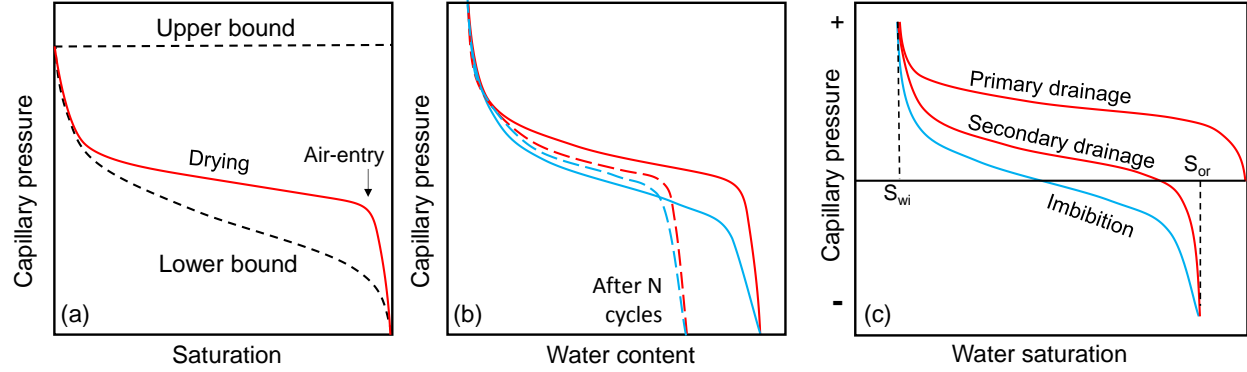


Figure 6. Pressure-saturation characteristic curve. (a) Typical trend and bounds. (b) Hysteretic behavior and asymptotic trend after N cycles and associated volume changes. (c) Change in wettability.

Spatial Distribution, Volumetric Strains and Hysteresis. Pore network topology, short-term instabilities and long-term fluid migration through the vapor phase lead to a non-homogenous distribution of defending and invading fluids.

Percolation. The moment when a fluid phase forms a continuous path between inlet and outlet defines the percolation saturation. Percolating paths are fractal and ensuing material properties are specimen-size dependent.

Spatial variability. The wetting fluid tends to remain in regions surrounded by small pores (e.g., water in silts next to sands), while hydrates nucleate preferentially within large pores (e.g., sand layers in fine-coarse stratigraphies). Spatial variability and correlation have a pronounced effect on the evolution of mixed-fluid conditions, hinder environmental remediation and leave behind either trapped or bypassed oil and gas during resource recovery [Le et al., 2012].

Patchiness. Often isolated, non-percolating “patches” rather than homogeneously distributed fluids should be expected between percolation thresholds and in the pendular regime. Patchy distribution results in transport and mechanical properties that are different to those when phases are homogeneously-randomly distributed [Dai et al., 2012; Dai and Santamarina, 2013].

Fines migration. Fines may migrate with the interface between immiscible fluids and accumulate at pore throats and at interparticle contacts (e.g., clay grains form stabilizing bridges between sandy grains in loess). Clogging of pore throats favor the formation of an internal vuggy structure during gas exsolution, and gas-driven fractures during desiccation [Jung et al., 2012].

Plastic strains and pore structure. Changes in suction s associated to changes in saturation S cause plastic volumetric strains ε_v and disturbs the pore structure, the degree of saturation and the pressure-saturation characteristic curve [Kodikara et al., 1999; Gallipoli et al., 2003; Wheeler et al., 2003; Khalili et al., 2008; Tarantino, 2009].

$$dS = \frac{\partial S}{\partial s} ds + \frac{\partial S}{\partial \varepsilon_v} d\varepsilon_v$$

Figure 6b presents the characteristic curve for a constant porous structure and for the same medium when fabric changes take place.

Hysteresis. The characteristic curve shows hysteretic behavior during wetting and drying, in part due to contact angle hysteresis, the non-homogeneous spatial distribution of fluids, plastic strains and fines migration addressed above (Figure 6b). Other pore-scale processes involved in hysteresis include: the “ink-bottle” effect when large pore bodies are connected through small pore throats, capillary condensation, entrapped air, and changes in pore structure caused by the precipitation of insoluble phases.

Time: From Diffusion to Dynamics. The standard capillary pressure-saturation relationship presumes thermodynamic equilibrium. However, measurements are often conducted in short-time laboratory scales. Gas diffusion plays a critical role on long-term pore filling and changes in saturation with time [Sun et al., 2017]. Furthermore, non-equilibrium conditions develop during advective regimes, and pressure-saturation trends become flow-rate dependent [Diamantopoulos et al., 2012; Hassanizadeh et al., 2002]. The saturation of the wetting fluid at a given capillary pressure increases with the velocity of the invading non-wetting fluid.

Changes in Wettability. The relative preference between fluids and a solid substrate may change over time. In fact, while most minerals are water wet, they may become oil-wet or mixed-wet during the life of the reservoir due to the adsorption or precipitation of organic molecules onto the mineral surface [Anderson, 1986; Buckley et al., 1998]. Therefore, the capillary pressure $\Delta u = u_{oil} - u_{water}$ is positive $\Delta u > 0$ during oil invasion (i.e., reservoir formation), but becomes negative $\Delta u < 0$ when the process is reversed (i.e., during oil production – Figure 6c). Wettability can be characterized from spontaneous and forced water imbibition or drainage [Morrow, 1990; Abdallah et al., 2007].

GAS INVASION VS. INTERNAL GAS NUCLEATION

Typically, the immiscible fluid invades from the boundary and remains a continuous phase. However, this is not always the case: gas can nucleate inside the porous medium and form isolated bubbles (e.g., bio-mediated gas nucleation, microbial decomposition of organic matter, depressurization and gas exsolution, hydrate dissociation). Similarly, isolated hydrate crystals nucleate inside sediments.

Gas Pressure. Consider gas either invading or nucleating inside a water-saturated sediment. In both cases: (1) the interfacial membrane wets grains and resists the advancing gas front, (2) grains are pulled back away from the advancing gas front, (3) the effective stress acting on grains that have been invaded by the gas phase is lower than the effective stress in the water-saturated grains, and (4) the capillary pressure $\Delta u = u_{gas} - u_{water} > 0$. However, while gas and liquid pressures are boundary-controlled during invasion, only the liquid pressure is boundary-controlled during internal gas nucleation (Figure 7).

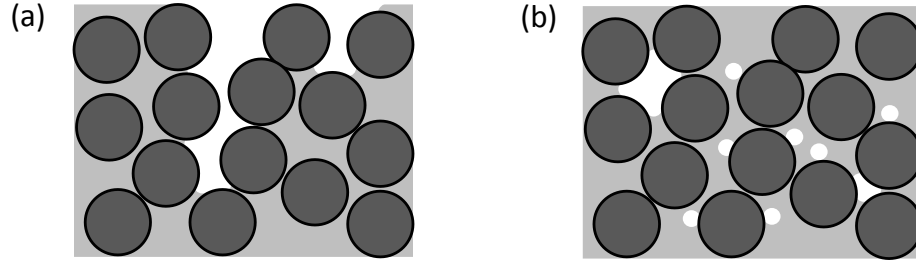


Figure 7. Unsaturation by (a) gas invasion and (b) internal gas nucleation

Preferential nucleation takes place in larger pores. Bubble growth after nucleation is limited by the pore throats that surround a given bubble. Therefore, different bubbles will have different transient gas pressures, contrary to the constant gas pressure in gas invasion. Eventually, bubbles become much larger than the grain size, encounter a similar statistical distribution of pore throats, and develop similar gas pressures even while they remain isolated [Jang and Santamarina, 2011, 2014].

The isolated gas phase may form (1) displacive gas bubbles without sediments inside (high air entry value sediment subjected to low effective stress), or (2) sediment-filled gas patches (either low gas entry value and/or high effective stress).

Physical Properties. Gas invasion and internal gas nucleation result in distinctly different mixed-fluid patterns within the porous medium. Ensuing differences in physical properties follow.

Pressure-saturation characteristic curve. Let's assume a single capillary pressure for all gas patches, and compare the ensuing capillary pressure vs. saturation curves obtained in gas nucleation and in gas invasion. Numerical results obtained using pore network modeling with constant pore structure show similar trends in both cases [Jang and Santamarina, 2014].

Relative permeabilities. The trends for relative gas and water permeabilities vs. saturation are also very similar, except for a lower gas permeability in gas nucleation than in invasion near the percolation threshold [Jang and Santamarina, 2014].

Bulk stiffness – P-wave velocity. The bulk stiffness of water-gas mixtures decreases rapidly as the gas content increases [Sills et al., 1991; analysis in Santamarina et al., 2001]. In the case of gas nucleation, the analysis must consider the gas pressure in isolated bubbles or gas patches, and its effect on the gas bulk stiffness κ_b :

$$\kappa_b = \frac{2T_s}{3r} \text{ (Bulk stiffness of gas bubbles)}$$

Therefore, the bulk stiffness of a fluid κ_f such as water κ_w in the presence of gas bubbles is

$$\kappa_f = \frac{1}{S \frac{1}{\kappa_w} + (1-S) \frac{3 \cdot r}{2 \cdot T_s}}$$

where S is the water saturation. Changes in saturation are readily detected using P-wave velocity measurements [Rebata-Landa and Santamarina, 2012].

Consolidation. Displacive gas bubbles (i.e., no sediments inside) readily contract in response to changes in confinement and cause immediate volume compaction. Note: contraction is limited by stress arching around bubbles [Sills et al., 1991; Puzrin et al., 2011]. Later, gas dissolution into the liquid and pressure diffusion or consolidation contribute to time-dependent volume contraction.

Shear strength. The internal nucleation of gas bubbles weakens the shear strength of soils [Sills et al., 1991; Sills and Wheeler, 1992]. On the one hand, displacive gas bubbles have no shear strength. On the other hand, sediments trapped in gas patches experience a lower effective stress than the surrounding water-saturated sediment and contribute a proportionally lower shear strength.

INTERPARTICLE FORCES - OPEN MODE DISCONTINUITIES

The forces between grains in a granular packing saturated by a single phase fluid system respond to effective stresses imposed at the boundaries. However, a new contribution to interparticle forces emerges when the granular medium is filled with a mixed fluid (Olivier Coussy's valuable contributions to unsaturated poroelasticity and crystallization are documented in Coussy, 2010, Coussy and Monteiro, 2007, Coussy, 2007, Coussy and Brisard, 2009).

Capillary Forces. The interfacial membrane hangs on to grain surfaces, and transfers its interfacial tension to each grain. In turn, the grain transfers this new force F_{cap} to the granular skeleton (Figure 8a). Therefore, the distribution of interparticle forces in a mixed fluid system depends both on the externally applied stresses and the internal distribution of the phases. The asymptotic solution for the interparticle contact force due to capillarity F_{cap} is [see also Cho and Santamarina, 2001]

$$F_{cap} = \pi d T_s$$

For comparison, the weight of the particle W scales with d^3 and skeletal forces N due to effective stress scale with d^2 . Therefore, capillary forces gain relevance for small particles d subjected to low effective stress σ' .

Clearly, the distribution of interparticle forces will be quite different for gas invasion and gas nucleation even at the same degree of saturation. From this perspective, effective stress concepts and constitutive models must be carefully constructed to address these distinct conditions.

Open Mode Discontinuities. Capillary forces cause particle displacement and changes in the pore structure. The most common observation is the volume contraction associated to the increase in suction. Open mode discontinuities develop when capillary forces F_{cap} exceed skeletal forces N induced by the effective stress imposed at boundaries (Figure 8b). As noted above, this should be expected in fine grained sediments with high air entry value and subjected to low effective stress, under both invasion and nucleation conditions.

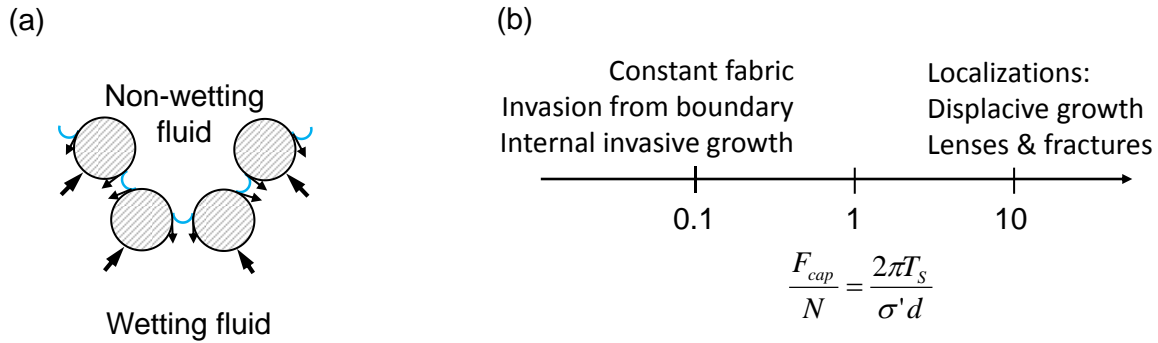


Figure 8. Capillary forces and hydro-mechanical coupling. (a) Intergranular capillary forces. (b) Open mode discontinuities in fine grained granular materials subjected to low effective stress.

Invasion: Desiccation Cracks. The decrease of water content causes the increase of capillary suction and consolidation of porous media. As the suction increases further, the air-water interface invades the largest pores and causes particle displacement away from the invasion point. As a result, the void ratio at the crack tip increases and the crack propagates. It should be noted that the effective stress is in compression everywhere during the crack initiation and propagation [Shin and Santamarina, 2010; Shin and Santamarina, 2011a,b]. A similar situation takes place in other systems, such as at the contact between a water-saturated clay and CO₂ [Espinoza and Santamarina, 2012].

Internal nucleation: from displacive bubbles to fractures (of from nodules to lenses). Similarly, internal nucleation such as gas exsolution can displace grains, as noted above. Enlarging cavities evolve into opening-mode fractures that are aligned transversely to the minimum effective stress. The nucleation and growth of other immiscible phases follow similar patterns, starting as nodules and eventually forming lenses; examples include hydrate bearing clayey sediments, frozen ground, and mineral precipitates.

SUMMARY

Mixed fluid conditions give rise to a wide range of phenomena in porous media. These phenomena and emergent processes have profound implications in soil-atmosphere interaction, energy geotechnology related to oil and gas recovery, CO₂ geological storage and environmental contamination/remediation.

Even the basic concepts of surface tension and contact angle require careful analyses. Surface tension depends on pressure (in gas-liquid systems), temperature, changes in solute concentration, and surfactant concentration. Contact angle responds to interfacial tensions, surface topography (it may exhibit a range of values at edges), invasion velocity, and chemical fluid-substrate interactions (it may change with time). Interfaces are not isolated, but they interact through the fluid pressure in response to external fields such as gravity.

The idealized cylindrical representation of pores fails to capture important capillarity effects. The converging-diverging geometry of pore throats *-longitudinal variation-* causes jumps

and snap-off instabilities. Surfactants may experience transient changes in surface density during dynamic events and the capillary response across a pore constriction will deviate from the signature anticipated for quasi-static conditions. Corners and edges -*cross-section*- favor the percolation of wetting liquids.

Ubiquitous pore-scale instabilities compound with macroscale instabilities associated to viscous and capillary effects to intensify fluid trapping. The spatial variability and correlation in the pore structure aggravates this situation. Consequently, instabilities and spatial variability diminish the recovery efficiency.

The saturation-pressure characteristic curve is saturation-history and flow-rate dependent, it is coupled with the mechanical response of the porous medium through changes in pore-structure, and it may change with time as a consequence of fluid-substrate reactions and long-term diffusion. Its hysteretic response gradually evolves towards a terminal condition when the medium is subjected to multiple wetting-drying cycles.

Time emerges as an important variable in mixed-fluid conditions. Common quasi-static analyses fail to capture the consequences of chemical reactions and rate processes, viscous effects, and long-term diffusive transport.

There are salient differences between unsaturation by internal gas nucleation and gas invasion, and the ensuing physical properties of the porous medium. Gas bubbles are isolated and may have different gas pressures, interparticle forces decrease and the porous medium tends to expand during internal gas nucleation. During gas invasion, the gas phase is continuous and it has the same pressure, capillary forces add to interparticle forces and the porous medium tends to contract. Open mode discontinuities may develop in both cases when the capillary entry pressure is high relative to the effective stress: displacive bubbles grow to form internal fractures during internal gas nucleation, and desiccation cracks form during gas invasion.

Notation

Δu	Capillary pressure [Pa]
ε_v	Volumetric strain []
κ	Bulk stiffness [Pa]. Subscripts: <i>b</i> = bubble, <i>f</i> = pore fluid, <i>w</i> = water
μ	Viscosity [Pa s]
θ	Contact angle [°]. Subscripts: <i>adv</i> = advancing, <i>rec</i> = receding
ρ	Density [kg/m ³]
σ'	Effective stress [Pa]
Ω	Molecular volume [m ³]
A_{eff}	The cross-section area of the non-wetting fluid [m ²]
Ca	Capillary number []
C_S	Spreading coefficient [N/m]
d	Particle size [m]
F_{cap}	Capillary force [N]
k_B	Boltzmann constant [J/K]
M	Viscosity ratio []

N	Skeleton force [m]
p_γ	Perimeter of contact line between the non-wetting fluid and the wetting fluid [m]
p_s	Perimeter of contact line between the nonwetting fluid and the solid [m]
r	Radius of the meniscus [m]
s	Suction [Pa]
S	Degree of saturation []
t	Time [s]
T	Temperature [K]
T_S	Surface or interfacial tension [N/m]. Subscripts: LS= liquid-solid, LV= liquid-vapor, and VS=vapor-solid
u	Fluid pressure [Pa]. Subscripts: L= liquid, sat= saturated vapor pressure, V= vapor.
v	Flow velocity [m/s]
w	Water content []
W	Weight of particle [N]

Acknowledgements: Support for this research was provided by the KAUST endowment. Gabrielle E. Abelskamp edited the manuscript.

REFERENCES

- Abdallah, W., Buckley, J. S., Carnegie, A., Edwards, J., Herold, B., Fordham, E., Graue, A., Habashy, T., Seleznev, N., Signer, C., Montaron, B., Hussain, H., & Ziauddin, M. (2007). Fundamentals of wettability. *Oilfield Review*, 19(2), 44-61.
- Alvarells, J. (2003). *Fundamental Studies of Capillary Forces in Porous Media*. Georgia Tech, Atlanta.
- Anderson, W. (1986). Wettability literature survey-part 1: Rock/oil/brine interactions and the effects of core handling on wettability. *Journal of Petroleum Technology*, 38(11), 1-246.
- Arriola, A., Willhite, G. P., & Green, D. W. (1983). Trapping of oil drops in a noncircular pore throat and mobilization upon contact with a surfactant. *Society of Petroleum Engineers Journal*, 23(01), 99-114.
- Berg, S., Ott, H., Klapp, S. A., Schwing, A., Neiteler, R., Brussee, N., Makurat, A., Leu, L., Enzmann, F., Schwarz, J., Kersten, M., Irvine, S., & Stampanoni, M. (2013). Real-time 3D imaging of Haines jumps in porous media flow. *Proceedings of the National Academy of Sciences*, 110(10), 3755-3759.
- Bico, J., & Quéré, D. (2002). Rise of liquids and bubbles in angular capillary tubes. *Journal of colloid and Interface Science*, 247(1), 162-166.
- Blake, T. D. (2006). The physics of moving wetting lines. *Journal of Colloid and Interface Science*, 299(1), 1-13.
- Blunt, M., Zhou, D., & Fenwick, D. (1995). Three-phase flow and gravity drainage in porous media. In *Multiphase Flow in Porous Media* (pp. 77-103). Springer Netherlands.
- Brooks, R. H., & Corey, A. T. (1964). Hydraulic properties of porous media and their relation to drainage design. *Trans. ASAE*, 7(1), 0026-0028.

- Buckley, J. S. (2001). Effective wettability of minerals exposed to crude oil. *Current opinion in colloid & interface science*, 6(3), 191-196.
- Buckley, J. S., & Liu, Y. (1998). Some mechanisms of crude oil/brine/solid interactions. *Journal of Petroleum Science and Engineering*, 20(3), 155-160.
- Butt, H., Graf, K., & Kappl, M. (2003). *Physics and chemistry of interfaces*. WILEY-VCH GmbH & Co. KGaA, Weinheim
- Camuffo, D. (1984). Condensation-evaporation cycles in pore and capillary systems according to the Kelvin model. *Water, Air, and Soil Pollution*, 21(1-4), 151-159.
- Chalraud, C., Robin, M., Lombard, J. M., Martin, F., Egermann, P., & Bertin, H. (2009). Interfacial tension measurements and wettability evaluation for geological CO₂ storage. *Advances in Water Resources*, 32(1), 98-109.
- Cho, G. C., & Santamarina, J. C. (2001). Unsaturated particulate materials—particle-level studies. *Journal of geotechnical and geoenvironmental engineering*, 127(1), 84-96.
- Choi, D., Lee, H., Kang, I. S., Lim, G., Kim, D. S., & Kang, K. H. (2013). Spontaneous electrical charging of droplets by conventional pipetting. *Scientific reports*, 3, 2037.
- Clements, J. A., Brown, E. S., & Johnson, R. P. (1958). Pulmonary surface tension and the mucus lining of the lungs: some theoretical considerations. *J. of app. physiology*, 12(2), 262-268.
- Coussy, O. (2007). Revisiting the constitutive equations of unsaturated porous solids using a Lagrangian saturation concept. *International Journal for Numerical and Analytical Methods in Geomechanics*, 31(15), 1675-1694.
- Coussy, O., & Monteiro, P. (2007). Unsaturated poroelasticity for crystallization in pores. *Computers and geotechnics*, 34(4), 279-290.
- Coussy, O., & Brisard, S. (2009). Prediction of drying shrinkage beyond the pore isodeformation assumption. *Journal of Mechanics of Materials and Structures*, 4(2), 263-279.
- Coussy, O. (2010). *Mechanics and physics of porous solids*. John Wiley & Sons, Ltd. Chichester, UK.
- Dai, S., & Santamarina, J. C. (2013). Water retention curve for hydrate - bearing sediments. *Geophysical Research Letters*, 40(21), 5637-5641.
- Dai, S., Santamarina, J. C., Waite, W. F., & Kneafsey, T. J. (2012). Hydrate morphology: Physical properties of sands with patchy hydrate saturation. *Journal of Geophysical Research: Solid Earth*, 117, B11205.
- De Gennes, P. G., Brochard-Wyart, F., & Quéré, D. (2004). *Capillarity and wetting phenomena: drops, bubbles, pearls, waves*. Springer Science & Business Media, New York
- Diamantopoulos, E., & Durner, W. (2012). Dynamic nonequilibrium of water flow in porous media: A review. *Vadose Zone Journal*, 11(3).
- Dong, M., & Chatzis, I. (1995). The imbibition and flow of a wetting liquid along the corners of a square capillary tube. *Journal of colloid and interface science*, 172(2), 278-288.
- Drummond, C., & Israelachvili, J. (2004). Fundamental studies of crude oil–surface water interactions and its relationship to reservoir wettability. *Journal of Petroleum Science and Engineering*, 45(1), 61-81.

- Espinoza, D. N., & Santamarina, J. C. (2010). Water - CO₂ - mineral systems: Interfacial tension, contact angle, and diffusion—Implications to CO₂ geological storage. *Water resources research*, 46, W03537.
- Espinoza, D. N., & Santamarina, J. C. (2012). Clay interaction with liquid and supercritical CO₂: the relevance of electrical and capillary forces. *International Journal of Greenhouse Gas Control*, 10, 351-362.
- Francisca, F. M., Rinaldi, V. A., & Santamarina, J. C. (2003). Instability of hydrocarbon films over mineral surfaces: Microscale experimental studies. *Journal of environmental engineering*, 129(12), 1120-1128.
- Fredlund, D. G. (2000). The 1999 RM Hardy Lecture: The implementation of unsaturated soil mechanics into geotechnical engineering. *Canadian Geotechnical Journal*, 37(5), 963-986.
- Gallipoli, D., Gens, A., Sharma, R., & Vaunat, J. (2003). An elasto-plastic model for unsaturated soil incorporating the effects of suction and degree of saturation on mechanical behaviour. *Géotechnique*, 53(1), 123-136.
- Gauglitz, P. A., & Radke, C. J. (1989). Dynamics of Haines jumps for compressible bubbles in constricted capillaries. *AIChE journal*, 35(2), 230-240.
- Hassanzadeh, S. M., Celia, M. A., & Dahle, H. K. (2002). Dynamic effect in the capillary pressure–saturation relationship and its impacts on unsaturated flow. *Vadose Zone Journal*, 1(1), 38-57.
- Holmberg, K., B. Jansson, B. Kronberg and B. Lindman (2003), *Surfactants and Polymers in Aqueous Solution*, John Wiley & Sons, Ltd, Chichester, UK.
- Hsu, S. Y., & Hilpert, M. (2015). Pore-scale visualization of the mobilization of a partially wetting droplet. *Advances in Water Resources*, 95, 235-245.
- Israelachvili, J. N. (2011), *Intermolecular and Surface Forces*, Academic Press, San Diego, CA.
- Jang, J., & Santamarina, J. C. (2011). Recoverable gas from hydrate - bearing sediments: Pore network model simulation and macroscale analyses. *Journal of geophysical research: Solid Earth*, 116(B8).
- Jang, J., & Santamarina, J. C. (2014). Evolution of gas saturation and relative permeability during gas production from hydrate - bearing sediments: Gas invasion vs. gas nucleation. *Journal of Geophysical Research: Solid Earth*, 119(1), 116-126.
- Jang, J., Sun, Z., & Santamarina, J. C. (2016). Capillary pressure across a pore throat in the presence of surfactants. *Water Resources Research*, 52, 9586–9599.
- Jasper, J. J. (1972). The surface tension of pure liquid compounds. *Journal of physical and chemical reference data*, 1(4), 841-1010.
- Jung, J. W., Jang, J., Santamarina, J. C., Tsouris, C., Phelps, T. J., & Rawn, C. J. (2012). Gas production from hydrate-bearing sediments: the role of fine particles. *Energy & Fuels*, 26(1), 480-487.
- Kalikmanov, V. (2013). *Nucleation theory* (Vol. 860). Springer. Netherlands.

- Karapetsas, G., Sahu, K. C., Sefiane, K., & Matar, O. K. (2014). Thermocapillary-driven motion of a sessile drop: effect of non-monotonic dependence of surface tension on temperature. *Langmuir*, 30(15), 4310-4321.
- Khalili, N., Habte, M. A., & Zargarbashi, S. (2008). A fully coupled flow deformation model for cyclic analysis of unsaturated soils including hydraulic and mechanical hystereses. *Computers and Geotechnics*, 35(6), 872-889.
- Kodikara, J., Barbour, S. L., & Fredlund, D. G. (1999). Changes in clay structure and behaviour due to wetting and drying. In *Proceedings 8th Australia New Zealand Conference on Geomechanics: Consolidating Knowledge* (p. 179). Australian Geomechanics Society.
- Kovscek, A. R., Wong, H., & Radke, C. J. (1993). A Pore-Level Scenario for the Development of Mixed Wettability in Oil Reservoirs. *AIChE Journal*, 39(6), 1073.
- Lago, M., & Araujo, M. (2001). Threshold pressure in capillaries with polygonal cross section. *Journal of colloid and interface science*, 243(1), 219-226.
- Le, T. M. H., Gallipoli, D., Sanchez, M., & Wheeler, S. J. (2012). Stochastic analysis of unsaturated seepage through randomly heterogeneous earth embankments. *International Journal for Numerical and Analytical Methods in Geomechanics*, 36(8), 1056-1076.
- Lenormand, R., Touboul, E., & Zarcone, C. (1988). Numerical models and experiments on immiscible displacements in porous media. *Journal of fluid mechanics*, 189, 165-187.
- Lenormand, R., Zarcone, C., & Sarr, A. (1983). Mechanisms of the displacement of one fluid by another in a network of capillary ducts. *Journal of Fluid Mechanics*, 135, 337-353.
- Ma, S., Mason, G., & Morrow, N. R. (1996). Effect of contact angle on drainage and imbibition in regular polygonal tubes. *Colloids and Surfaces A: Physicochemical and Engineering Aspects*, 117(3), 273-291.
- Mason, G., & Morrow, N. R. (1991). Capillary behavior of a perfectly wetting liquid in irregular triangular tubes. *Journal of Colloid and Interface Science*, 141(1), 262-274.
- Mason, G., & Morrow, N. R. (1994). Effect of contact angle on capillary displacement curvatures in pore throats formed by spheres. *J. of colloid and interface science*, 168(1), 130-141.
- Massoudi, R., & King Jr, A. D. (1974). Effect of pressure on the surface tension of water. Adsorption of low molecular weight gases on water at 25. deg. *The Journal of Physical Chemistry*, 78(22), 2262-2266.
- Mohanty, K. K., Davis, H. T., & Scriven, L. E. (1987). Physics of oil entrapment in water-wet rock. *SPE Reservoir Engineering*, 2(01), 113-128.
- Morrow, N. R. (1970). Physics and thermodynamics of capillary action in porous media. *Industrial & Engineering Chemistry*, 62(6), 32-56.
- Morrow, N. R. (1990). Wettability and its effect on oil recovery. *Journal of Petroleum Technology*, 42(12), 1-476.
- Peña, T. J., Carvalho, M. S., & Alvarado, V. (2009). Snap - off of a liquid drop immersed in another liquid flowing through a constricted capillary. *AIChE journal*, 55(8), 1993-1999.
- Podgorski, T., Flesselles, J. M., & Limat, L. (2001). Corners, cusps, and pearls in running drops. *Physical Review Letters*, 87(3), 036102.

- Powers, S. E., & Tamblin, M. E. (1995). Wettability of porous media after exposure to synthetic gasolines. *Journal of Contaminant Hydrology*, 19(2), 105-125.
- Powers, S. E., Anckner, W. H., & Seacord, T. F. (1996). Wettability of NAPL-contaminated sands. *Journal of Environmental Engineering*, 122(10), 889-896.
- Puzrin, A. M., Tront, J., Schmid, A., & Hughes, J. B. (2011). Engineered use of microbial gas production to decrease primary consolidation settlement in clayey soils. *Géotechnique*, 61(9), 785-794.
- Quéré, D. (2008). Wetting and roughness. *Annu. Rev. Mater. Res.*, 38, 71-99.
- Ransohoff, T. C., & Radke, C. J. (1988a). Laminar flow of a wetting liquid along the corners of a predominantly gas-occupied noncircular pore. *Journal of Colloid and Interface Science*, 121(2), 392-401.
- Ransohoff, T. C., & Radke, C. J. (1988b). Mechanisms of foam generation in glass-bead packs. *SPE reservoir engineering*, 3(02), 573-585.
- Rebata-Landa, V., & Santamarina, J. C. (2012). Mechanical effects of biogenic nitrogen gas bubbles in soils. *J. Geotechnical and Geoenvironmental Engineering*, 138(2), 128-137.
- Roof, J. G. (1970). Snap-off of oil droplets in water-wet pores. *Society of Petroleum Engineers Journal*, 10(01), 85-90.
- Rosen, M. J. (2004), *Surfactants and Interfacial Phenomena*, John Wiley & Sons. Hoboken, NJ.
- Rossen, W. R. (2003). A critical review of Roof snap-off as a mechanism of steady-state foam generation in homogeneous porous media. *Colloids and Surfaces A: Physicochemical and Engineering Aspects*, 225(1), 1-24.
- Santamarina, J.C., in collaboration with Klein, K. and Fam, M. (2001). *Soils and Waves*, J. Wiley and Sons, Chichester, UK.
- Santamarina, J. C., & Jang, J. (2010). Energy geotechnology: Implications of mixed fluid conditions. In *International conference on unsaturated soils*, Sep. 6-8, Barcelona, Spain.
- Santos, L. P., Ducati, T. R., Balestrin, L. B., & Galembeck, F. (2011). Water with excess electric charge. *The Journal of Physical Chemistry C*, 115(22), 11226-11232.
- Shin, H., & Santamarina, J. C. (2010). Fluid-driven fractures in uncemented sediments: Underlying particle-level processes. *Earth and Planetary Science Letters*, 299(1), 180-189.
- Shin, H., & Santamarina, J. C. (2011a). Desiccation cracks in saturated fine-grained soils: particle-level phenomena and effective-stress analysis. *Géotechnique*, 61(11), 961-972.
- Shin, H., & Santamarina, J. C. (2011b). Open-mode discontinuities in soils. *Géotechnique Letters*, 1(4), 95-99.
- Sills, G. C., & Wheeler, S. J. (1992). The significance of gas for offshore operations. *Continental Shelf Research*, 12(10), 1239-1250.
- Sills, G. C., Wheeler, S. J., Thomas, S. D., & Gardner, T. N. (1991). Behaviour of offshore soils containing gas bubbles. *Geotechnique*, 41(2), 227-241.
- Snoeijer, J. H., & Andreotti, B. (2013). Moving contact lines: scales, regimes, and dynamical transitions. *Annual review of fluid mechanics*, 45, 269-292.

- Sobolev, V. D., Churaev, N. V., Velarde, M. G., & Zorin, Z. M. (2000). Surface tension and dynamic contact angle of water in thin quartz capillaries. *Journal of colloid and interface science*, 222(1), 51-54.
- Sun, Z., Jang, J. and Santamarina, J.C. (2017). Long-term pore filling – Implications in reservoir formation and resource recovery. Submitted for publication – Available from the authors.
- Tarantino, A. (2009). A water retention model for deformable soils. *Géotechnique*, 59(9), 751-762.
- Van Genuchten, M. T. (1980). A closed-form equation for predicting the hydraulic conductivity of unsaturated soils. *Soil science society of America journal*, 44(5), 892-898.
- Wardlaw, N. C. (1982). The effects of geometry, wettability, viscosity and interfacial tension on trapping in single pore-throat pairs. *J. Canadian Petroleum Technology*, 21(03), 21-27
- Weissenborn, P. K., & Pugh, R. J. (1996). Surface tension of aqueous solutions of electrolytes: relationship with ion hydration, oxygen solubility, and bubble coalescence. *Journal of Colloid and Interface Science*, 184(2), 550-563.
- Wheeler, S. J., Sharma, R. S., & Buisson, M. S. R. (2003). Coupling of hydraulic hysteresis and stress–strain behaviour in unsaturated soils. *Géotechnique*, 53(1), 41-54.
- Yu, L., & Wardlaw, N. C. (1986a). The influence of wettability and critical pore-throat size ratio on snap—off. *Journal of Colloid and Interface Science*, 109(2), 461-472.
- Yu, L., & Wardlaw, N. C. (1986b). Mechanisms of nonwetting phase trapping during imbibition at slow rates. *Journal of colloid and interface science*, 109(2), 473-486.
- Zhang, C., Oostrom, M., Wietsma, T. W., Grate, J. W., & Warner, M. G. (2011). Influence of viscous and capillary forces on immiscible fluid displacement: Pore-scale experimental study in a water-wet micromodel demonstrating viscous and capillary fingering. *Energy & Fuels*, 25(8), 3493-3505.
- Zhou, D., & Blunt, M. (1997). Effect of spreading coefficient on the distribution of light non-aqueous phase liquid in the subsurface. *Journal of Contaminant Hydrology*, 25(1-2), 1-19.